Topologically Nontrivial Valley States in Bilayer Graphene Quantum Point Contacts

Hiske Overweg,[1] Angelika Knothe,[2] Thomas Fabian,[3] Lukas Linhart,[3] Peter Rickhaus,[1,*] Lucien Wernli,[1] Kenji Watanabe,[4] Takashi Taniguchi,[4] David Sánchez,[5] Joachim Burgdörfer,[3] Florian Libisch,[3] Vladimir I. Fal'ko,[2] Klaus Ensslin,[1] and Thomas Ihn[1]

[1]*Solid State Physics Laboratory, ETH Zürich, CH-8093 Zürich, Switzerland*
[2]*National Graphene Institute, University of Manchester, Manchester M13 9PL, United Kingdom*
[3]*Institute for Theoretical Physics, Vienna University of Technology, A-1040 Vienna, Austria*
[4]*National Institute for Material Science, 1-1 Namiki, Tsukuba 305-0044, Japan*
[5]*Institute for Cross-Disciplinary Physics and Complex Systems IFISC (UIB-CSIC), 07122 Palma de Mallorca, Spain*

(Received 6 September 2018; published 20 December 2018)

We present measurements of quantized conductance in electrostatically induced quantum point contacts in bilayer graphene. The application of a perpendicular magnetic field leads to an intricate pattern of lifted and restored degeneracies with increasing field: at zero magnetic field the degeneracy of quantized one-dimensional subbands is four, because of a twofold spin and a twofold valley degeneracy. By switching on the magnetic field, the valley degeneracy is lifted. Because of the Berry curvature, states from different valleys split linearly in magnetic field. In the quantum Hall regime fourfold degenerate conductance plateaus reemerge. During the adiabatic transition to the quantum Hall regime, levels from one valley shift by two in quantum number with respect to the other valley, forming an interweaving pattern that can be reproduced by numerical calculations.

DOI: 10.1103/PhysRevLett.121.257702

Conductance quantization in one-dimensional channels is among the cornerstones of mesoscopic quantum devices. It has been observed in a large variety of material systems, such as n-type GaAs [1,2], p-type GaAs [3,4], SiGe [5], GaN [6], InSb [7], AlAs [8], and Ge [9]. Typically spin degeneracy leads to quantization in multiples of $2e^2/h$. In single and bilayer graphene both steps of $2e^2/h$ and $4e^2/h$ have been reported [10–15], although a fourfold degeneracy is expected due to the additional valley degree of freedom. Here we present data for three quantum point contacts (QPCs) which display (approximately) fourfold degenerate modes both at zero magnetic field and in the quantum Hall regime, and twofold degenerate modes in the transition region. The Berry curvature in gapped bilayer graphene induces an orbital magnetic moment for the states selected by the quantum point contact [16]. The valleys therefore split linearly in a weak magnetic field and conductance steps of $2e^2/h$ emerge. The adiabatic evolution of conduction steps to the quantum Hall regime reveals a universal level crossing pattern: state energies in one valley shift by two with respect to those of the other valley due to the chirality of the effective low-energy Hamiltonian in the K_+ and K_- valley, a general feature of Dirac particles in even spatial dimensions [17]. Related topological effects involving the valley degree of freedom have recently been discussed in bilayer [16,18–22] and trilayer graphene [23]. The lifting and restoring of level degeneracies is explained in detail by two complementary theoretical models. These results are the basis for a detailed understanding of conductance quantization and tunneling barriers in bilayer graphene, enabling high-quality quantum devices.

The device geometry is similar to the one employed in our demonstration of full pinch-off of bilayer graphene quantum point contacts [15]. A bilayer graphene (BLG) flake was encapsulated between hexagonal boron nitride layers (hBN), using the van der Waals pick-up technique [24], and deposited onto a graphite flake [see Fig. 1(a) for a schematic of the final device geometry]. The graphene layer was contacted with Cr/Au contacts and a top gate pattern, consisting of six pairs of split gates (SG) with spacings ranging from 50 to 180 nm, was evaporated. On top of the device a layer of Al_2O_3 and finally the channel gates (CH) were deposited. An atomic force microscopy image of the sample, recorded prior to the deposition of the channel gates, is shown in Fig. 1(b). In the this Letter, we show data from three QPCs: QPC S (50 nm split gate separation), QPC M (80 nm), and QPC L (180 nm).

By applying voltages of opposite sign to the graphite back gate and the split gates, a displacement field between the two graphene layers is established, leading to the opening of a band gap [25]. In Ref. [15] we demonstrated that this suppresses transport below the split gates. Hence a

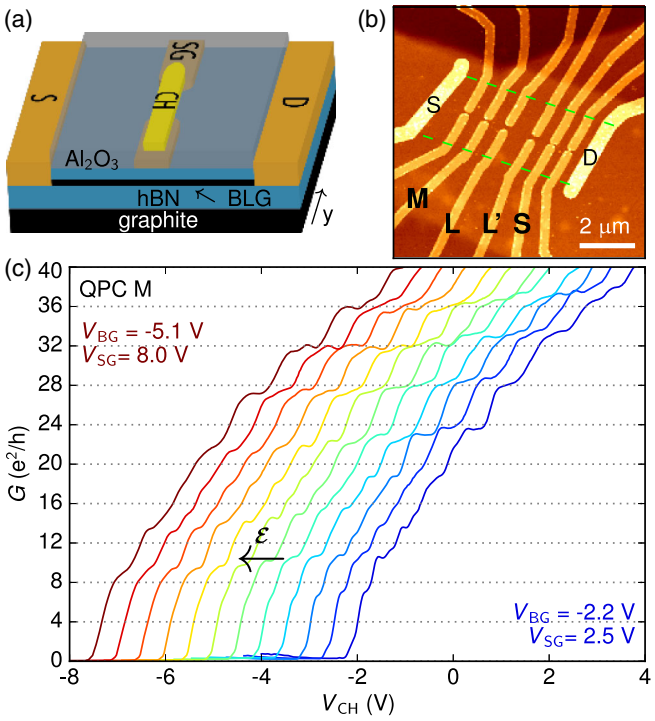

FIG. 1. (a) Schematic of the device consisting of bilayer graphene encapsulated in hBN on top of a graphite back gate. On top of the device split gates were evaporated. A layer of Al_2O_3 serves to separate the split gates from the channel gate. (b) Atomic force microscopy image of the device. Green dashed lines denote the edges of the bilayer graphene flake. Contacts are labeled S and D. Six pairs of split gates are situated between the contacts. (c) Conductance as a function of channel gate voltage for various combinations of the split gate and back gate voltage, showing conductance plateaus with a step size of $\Delta G = 4e^2/h$ for large quantum numbers.

constriction is formed, in which the charge carrier density can be tuned by the channel gate voltage. During the measurements, a large displacement field was applied beneath a single pair of split gates and the channel gate voltage was used to adjust the density and the displacement field $\mathcal{E}$ in the channel. The measurements were performed at $T = 1.7$ K.

The conductance of QPC M (80 nm wide) as a function of channel gate voltage is shown in Fig. 1(c) for various combinations of the split and back gate voltage. For each curve, a series resistance was subtracted, which corresponds to the resistance measured at the same back gate voltage with uniform charge carrier density throughout the sample. The traces show several plateaus with a typical step size of $\Delta G = 4e^2/h$, in particular for large quantum numbers, as previously reported in Ref. [15]. Similar results have been found for QPC L and L' (180 nm wide) with a smaller spacing in gate voltage between the plateaus, in agreement with the wider channel, and for QPC S (50 nm wide) with a larger spacing. For the employed range of gate voltages, the displacement field $\mathcal{E}$ does not significantly change the observed plateau sequence. Below $G = 24e^2/h$ we observe several kinks which cannot be identified as plateaus and some plateaus occurring below the expected conductance values. Reduced screening of the disorder potential in this low density regime might play a role. Simulations of the electrostatic potential [15] show that in this regime the confinement potential is shallow. From a theoretical perspective the nonmonotonicity of the dispersion relation, which becomes more pronounced for larger gaps and wider channels, can lead to additional degeneracies for low mode numbers, possibly explaining the absence of a plateau at $G = 4e^2/h$ [26].

The conductance of QPC M as a function of channel gate voltage for several magnetic field strengths [Fig. 2(a)] features a plateau sequence at $B = 0$ T described by $G = 4Ne^2/h$ with integer N. Increasing the magnetic field to a value of $B = 2.2$ T changes the plateau sequence to $G = 2Ne^2/h$. At $B = 5$ T the conventional sequence of Landau levels of BLG is observed, with $G = 4Ne^2/h$. In the lowest two Landau levels a lifting of the fourfold degeneracy can be observed. Around $B = 1.5$ T, during the transition to the Hall regime, the fourfold degeneracy is restored: the sequence is shifted to $G = (4N + 2)e^2/h$. This is most clearly visible for the modes for which $G \geq 22e^2/h$.

To further investigate this transition we inspect the transconductance as a function of channel gate voltage and magnetic field [see Fig. 2(b)]. Mode transitions show up as dark lines, which start out vertically in low magnetic fields, but bend toward more positive gate voltages above $B = 1$ T. This phenomenon, known as magnetic depopulation and observed, for instance, in high quality GaAs [27], is due to the transition from electrostatic confinement to magnetic confinement. What is unusual, however, is the pattern of mode splittings and mode crossings.

The same pattern can be observed for the wider QPCs [Fig. 2(c)], where the fourfold degeneracy is already restored at 2 T because of the wider channel. Although the lowest modes are hard to resolve, a robust pattern of mode crossings can be observed for many higher modes. Furthermore, we measured similar patterns for various displacement fields inside the channel and also for a p-doped channel (see the Supplemental Material [28], Secs. J and K).

To elucidate the evolution of the conductance steps with magnetic field, we simulate the experimental setup using two independent, complementary theoretical approaches, kp theory [25], and tight-binding calculations [29] (see the Supplement Material [28] for technical details). Both approaches agree well with each other and the experiment, highlighting the robustness of the observed features and the validity of our two modeling

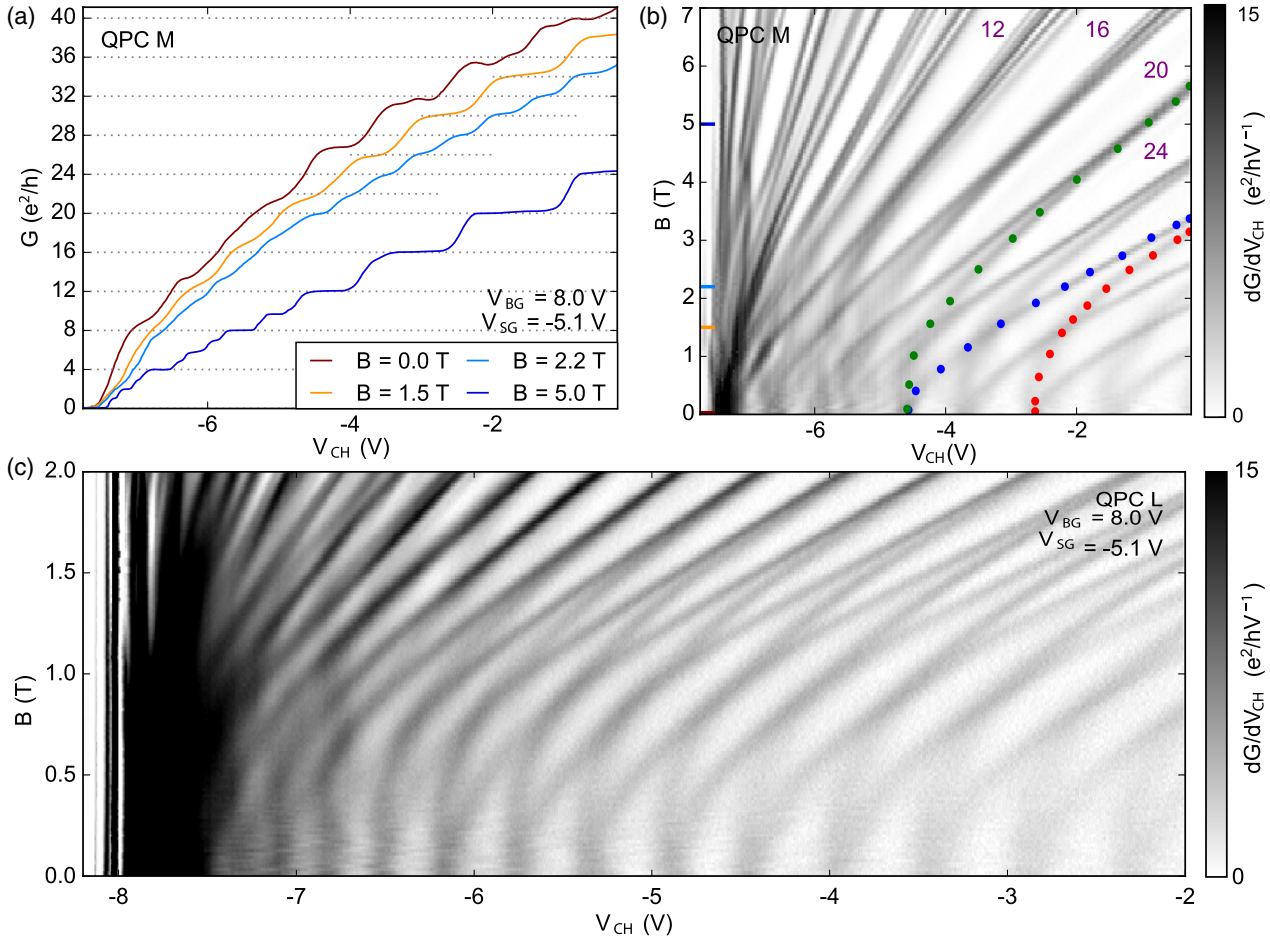

FIG. 2. (a) Conductance of QPC M as a function of V_{CH} for various magnetic field strengths. Several quantization sequences are observed. (b) Transconductance of QPC M as a function V_{CH} and magnetic field. A pattern of mode splittings (see green and blue dotted modes) is observed. Numbers in purple indicate the conductance values in the quantum Hall regime. (c) Transconductance of QPC L as a function V_{CH} and magnetic field. A similar pattern of mode crossings is observed in a smaller magnetic field range than for QPC M.

approaches. They reproduce and explain the observed low-field splitting (Fig. 3) and the level crossing pattern (Fig. 4).

Here, we use soft electrostatic confinement provided by a transverse electric field both at $B = 0$ and at a finite magnetic field. The obtained magnetic field dependence of the miniband edges represents the closest spectral analogue of the experimentally measured transconductance spectrum. We chose the potential landscape for kp theory by matching the mode spacing extracted from finite bias measurements of QPC M at $B = 0$ T (see Supplemental Material [28], Sec. L). Note that in the experiment the channel gate voltage influences not only the Fermi level, but also the shape of the confinement potential and the size of the displacement field inside the channel. To obtain one-to-one agreement between the calculation and the experimental results, a self-consistent potential would be required.

At zero magnetic field, we find spin- and valley-degenerate spectra [Fig. 3(a)] in agreement with the experimentally observed step size of $\Delta G = 4e^2/h$ [Fig. 2(a)]. The subband edges (for small mode numbers) are situated at finite momenta, reminiscent of the three minivalleys in gapped BLG in the presence of trigonal warping [25,30]. When switching on a magnetic field, the interlayer asymmetry leads to valley splitting of electron subbands, clearly seen in the band structure computed for $B = 2.2$ T [Fig. 3(b), blue and magenta subbands]. This lifting of valley degeneracy is in agreement with the measured step size of $\Delta G = 2e^2/h$ [see Fig. 2(a)]. The valley splitting is linear in B for small magnetic fields [see Fig. 3(b)]. This is related to the fact that the zero-field states of trigonally warped, gapped BLG [25,30] carry nontrivial Berry curvature and, consequently, a finite magnetic moment, M_z. We label the zero-field states $|n_\xi\rangle$, with transverse quantum number $n = 0, 1, \ldots$ in the K_ξ ($\xi = \pm$)

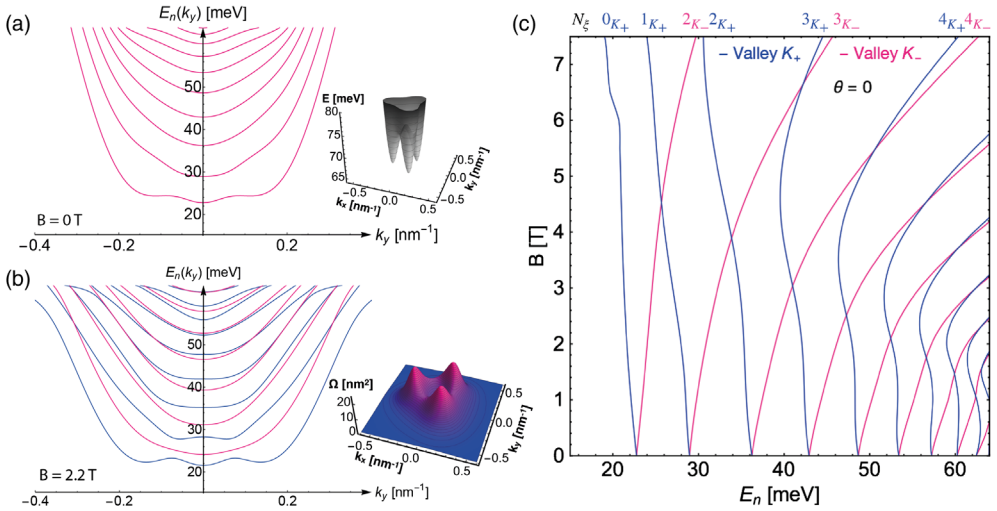

FIG. 3. (a) Band structure (conduction band) at $B = 0$ T of BLG in the presence of a confinement potential $U(x)$ and a modulated gap $\Delta(x)$ as described in the text showing a discrete, valley degenerate mode spectrum. Inset: lowest conduction band of homogeneous gapped BLG (K_- valley) for $\Delta_0 = 150$ meV with three minivalleys forming around the K point. (b) Band structure (conduction band) of the channel at $B = 2.2$ T, where symmetry between valleys is broken. The valley splitting at small magnetic fields is proportional to the magnetic field. Inset: Berry curvature Ω of the corresponding states with nonzero peaks in the three minivalleys. (c) Magnetic field dependence of the subband edges of the conduction bands in the electron channel. The nontrivial Berry curvature of the zero-field states implies a nonzero orbital magnetic moment M of the states, $M \propto \Omega$, which induces the linear in magnetic field splitting at small magnetic fields. At high magnetic fields the levels evolve into the LLs of gapped BLG.

valley. The Berry curvature can be seen in the inset of Fig. 3(b) and in Supplemental Material [28], Sec. B. For larger displacement fields, the Berry curvature becomes more spread out in k space around the K points, affecting several of the lowest modes.

In the high magnetic field regime, where the magnetic length is smaller than the channel width, the subbands in the channel become drifting states in the BLG Landau levels (LLs) $|N_\xi\rangle$, where N now indicates the LL index. The LL spectrum of BLG has a pair of special states $N = 0, 1$, that appear at zero energy in ungapped BLG with the wave functions residing on different layers in the opposite valleys. After the displacement field introduces a layer asymmetry gap, these states split apart by Δ, resulting in the two lowest conduction band subbands belonging to only one valley, e.g., K_+ (then, the highest valence band subbands would be from valley K_-). The other LLs in both valleys with $N \geq 2$ have approximately the same weight on the sublattices in the two layers and very close energies. Such an asymptotic behavior corresponds to the evolution of the subbands such that subbands $(n+2)_{K_+}$ eventually merge with subbands n_{K_-} upon an increase in magnetic field as shown in Fig. 4(a). For $B < 0$, the same pattern emerges with the two valleys interchanged [see Figs. 4(b) and 4(c)].

Note that the absence of hard edges characteristic for the present electrostatically defined bilayer constriction is critical for observing the interweaving pattern of crossing states. In rough-edged constrictions broken valley symmetry due to scattering quickly obscures the underlying pattern. These difficulties aside, a similar crossing pattern appears in principle in single layer graphene, as we have verified numerically for an ideal constriction (see Supplemental Material [28], Sec. H).

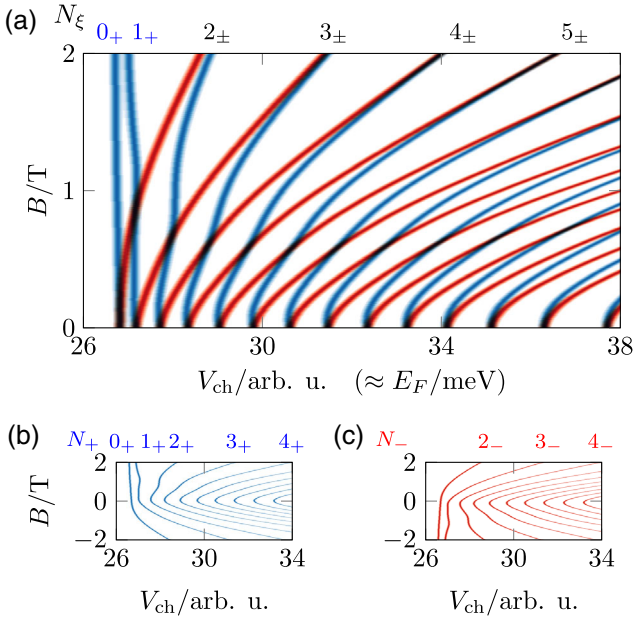

FIG. 4. (a) Differential conductance dG/dE of a 180 nm wide BLG nanoribbon, including a thermal smoothening of 1.7 K. (b) and (c) show separately the contributions from the two valleys K_+ and K_- at low energies. The channel voltage is determined through the relation $V_{CH} \propto \sqrt{E_F^2 - (\Delta/2)^2}$, with $\Delta/2 = 25$ meV.

In conclusion, we reported on the experimental observation of the mode crossing pattern during the evolution from size quantization to the Hall regime in BLG QPC. A valley splitting linear in magnetic field could be explained by a nontrivial orbital magnetic moment of states in gapped BLG. Our experimental results could be reproduced by numerical simulations.

We thank A. Rebhan for fruitful discussions. We acknowledge financial support from the European Graphene Flagship, the Swiss National Science Foundation via NCCR Quantum Science and Technology, ERC Synergy Hetero 2D, WWTF Project No. MA14-002, and MECD. Calculations were performed on the Vienna Scientific Cluster (VSC). Growth of hexagonal boron nitride crystals was supported by the Elemental Strategy Initiative conducted by MEXT, Japan and the CREST (JPMJCR15F3), JST, EC Project 2D·SIPC, Grant No. 820378.

Note added.—A closely related, complementary work has recently appeared [31].

*peterri@phys.ethz.ch

[1] B. J. Van Wees and H. Van Houten, Quantized Conductance of Point Contacts in a Two-Dimensional Electron Gas, Phys. Rev. Lett. **60**, 848 (1988).

[2] D. A. Wharam, T. J. Thornton, R. Newbury, M. Pepper, H. Ahmed, J. E. F. Frost, D. G. Hasko, D. C. Peacock, D. A. Ritchie, and G. A. C. Jones, One-dimensional transport and the quantisation of the ballistic resistance, J. Phys. C **21**, L209 (1988).

[3] L. P. Rokhinson, L. N. Pfeiffer, and K. W. West, Spontaneous Spin Polarization in Quantum Point Contacts, Phys. Rev. Lett. **96**, 156602 (2006).

[4] R. Danneau, W. R. Clarke, O. Klochan, A. P. Micolich, A. R. Hamilton, M. Y. Simmons, M. Pepper, and D. A. Ritchie, Conductance quantization and the $0.7 \times 2e2/h$ conductance anomaly in one-dimensional hole systems, Appl. Phys. Lett. **88**, 012107 (2006).

[5] D. Többen, D. A. Wharam, G. Abstreiter, J. P. Kotthaus, and F. Schäffler, Ballistic electron transport through a quantum point contact defined in a $\{Si/Si\{0.7\}Ge\{0.3\}\}$ heterostructure, Semicond. Sci. Technol. **10**, 711 (1995).

[6] H. T. Chou, S. Lüscher, D. Goldhaber-Gordon, M. J. Manfra, A. M. Sergent, K. W. West, and R. J. Molnar, High-quality quantum point contacts in GaN/AlGaN heterostructures, Appl. Phys. Lett. **86**, 073108 (2005).

[7] N. Goel, J. Graham, J. C. Keay, K. Suzuki, S. Miyashita, M. B. Santos, and Y. Hirayama, Ballistic transport in InSb mesoscopic structures, Physica (Amsterdam) **26E**, 455 (2005).

[8] O. Gunawan, B. Habib, E. P. De Poortere,, and M. Shayegan, Quantized conductance in an AlAs two-dimensional electron system quantum point contact, Phys. Rev. B **74**, 155436 (2006).

[9] R. Mizokuchi, R. Maurand, F. Vigneau, M. Myronov, and S. De Franceschi, Ballistic one-dimensional holes with strong g-factor anisotropy in germanium, Nano Lett. **18**, 4861 (2018).

[10] N. Tombros, A. Veligura, J. Junesch, M. H. D. Guimarães, I. J. Vera Marun, H. T. Jonkman, and B. J. van Wees, Quantized conductance of a suspended graphene nanoconstriction, Nat. Phys. **7**, 697 (2011).

[11] B. Terrés, L. A. Chizhova, F. Libisch, J. Peiro, D. Jörger, S. Engels, A. Girschik, K. Watanabe, T. Taniguchi, S. V. Rotkin, J. Burgdörfer, and C. Stampfer, Size quantization of Dirac fermions in graphene constrictions, Nat. Commun. **7**, 11528 (2016).

[12] M. Kim, J.-H. Choi, S.-H. Lee, K. Watanabe, T. Taniguchi, S.-H. Jhi, and H.-J. Lee, Valley-symmetry-preserved transport in ballistic graphene with gate-defined carrier guiding, Nat. Phys. **12**, 1022 (2016).

[13] M. T. Allen, J. Martin, and A. Yacoby, Gate-defined quantum confinement in suspended bilayer graphene, Nat. Commun. **3**, 934 (2012).

[14] A. S. M. Goossens, S. C. M. Driessen, T. A. Baart, K. Watanabe, T. Taniguchi, and L. M. K. Vandersypen, Gate-defined confinement in bilayer graphene-hexagonal boron nitride hybrid devices, Nano Lett. **12**, 4656 (2012).

[15] H. Overweg, H. Eggimann, X. Chen, S. Slizovskiy, M. Eich, P. Simonet, R. Pisoni, Y. Lee, K. Watanabe, T. Taniguchi, V. Fal'ko, K. Ensslin, and T. Ihn, Electrostatically induced quantum point contact in bilayer graphene, Nano Lett. **18**, 553 (2018).

[16] F. Zhang, J. Jung, G. A. Fiete, Q. Niu, and A. H. MacDonald, Spontaneous Quantum Hall States in Chirally Stacked Few-Layer Graphene Systems, Phys. Rev. Lett. **106**, 156801 (2011).

[17] A. N. Redlich, Parity violation and gauge noninvariance of the effective gauge field action in three dimensions, Phys. Rev. D **29**, 2366 (1984).

[18] M. Sui, G. Chen, L. Ma, W. Y. Shan, D. Tian, K. Watanabe, T. Taniguchi, X. Jin, W. Yao, D. Xiao, and Y. Zhang, Gate-tunable topological valley transport in bilayer graphene, Nat. Phys. **11**, 1027 (2015).

[19] A. Cortijo, F. Guinea, and M. A. H. Vozmediano, Geometrical and topological aspects of graphene and related materials, J. Phys. A **45**, 383001 (2012).

[20] K. S. Novoselov, E. McCann, S. V. Morozov, V. I. Fal'ko, M. I. Katsnelson, U. Zeitler, D. Jiang, F. Schedin, and A. K. Geim, Unconventional quantum Hall effect and Berry's phase of 2π in bilayer graphene, Nat. Phys. **2**, 177 (2006).

[21] C. N. R. Rao and A. K. Sood, *Graphene: Synthesis, Properties, and Phenomena* (Wiley, New York, 2013).

[22] B. J. Wieder, F. Zhang, and C. L. Kane, Critical behavior of four-terminal conductance of bilayer graphene domain walls, Phys. Rev. B **92**, 085425 (2015).

[23] T. Taychatanapat, K. Watanabe, T. Taniguchi, and P. Jarillo-Herrero, Quantum Hall effect and Landau-level crossing of dirac fermions in trilayer graphene, Nat. Phys. **7**, 621 (2011).

[24] L. Wang, I. Meric, P. Y. Huang, Q. Gao, Y. Gao, H. Tran, T. Taniguchi, K. Watanabe, L. M. Campos, D. A. Muller, J. Guo, P. Kim, J. Hone, K. L. Shepard, and C. R. Dean, One-dimensional electrical contact to a two-dimensional material, Science **342**, 614 (2013).

[25] E. McCann and V. I. Fal'ko, Landau-Level Degeneracy and Quantum Hall Effect in a Graphite Bilayer, Phys. Rev. Lett. **96**, 086805 (2006).

[26] A. Knothe and V. Fal'ko, Influence of minivalleys and Berry curvature on electrostatically induced quantum wires in gapped bilayer graphene, Phys. Rev. B **98**, 155435 (2018).

[27] B. J. van Wees, L. P. Kouwenhoven, H. van Houten, C. W. J. Beenakker, J. E. Mooij, C. T. Foxon, and J. J. Harris, Quantized conductance of magnetoelectric subbands in ballistic point contacts, Phys. Rev. B **38**, 3625 (1988).

[28] See Supplemental Material at http://link.aps.org/supplemental/10.1103/PhysRevLett.121.257702 for the model Hamiltonian, the description of bulk properties and numerical diagonalization inside the channel, the channel spectra for different parameters, details of the tight binding simulation, the effective low field hamiltonian, treatment of magnetic field and displacement field and calculations for monolayer graphene.

[29] F. Libisch, S. Rotter, and J. Burgdörfer, Coherent transport through graphene nanoribbons in the presence of edge disorder, New J. Phys. **14**, 123006 (2012).

[30] A. Varlet, D. Bischoff, P. Simonet, K. Watanabe, T. Taniguchi, T. Ihn, K. Ensslin, M. Mucha-Kruczyński, and V. I. Fal'ko, Anomalous Sequence of Quantum Hall Liquids Revealing a Tunable Lifshitz Transition in Bilayer Graphene, Phys. Rev. Lett. **113**, 116602 (2014).

[31] R. Kraft, I. V. Krainov, V. Gall, A. P. Dmitriev, R. Krupke, I. V. Gornyi, and R. Danneau, following Letter, Valley subband splitting in bilayer graphene quantum point contact, this issue, Phys. Rev. Lett. **121**, 257703 (2018).